Modeling geo-electric fields and geomagnetically induced currents (GIC) around New Zealand to explore GIC in the South Island's electrical transmission network

T. Divett[1], M. Ingham[2], C. D. Beggan[3], G. S. Richardson[3], C. J. Rodger[1], A. W. P. Thomson[3] and M. Dalzell[4]

[1]Department of Physics, University of Otago, Dunedin, New Zealand.
[2]Victoria University of Wellington, New Zealand.
[3]British Geological Survey, Edinburgh, UK.
[4]Transpower New Zealand Ltd., Wellington, New Zealand

Key Points:

- Developed a thin-sheet conductance model, electric field and GIC network models for New Zealand
- Strong electric fields on land aligned perpendicular to New Zealand's main axis for most B field directions
- GIC is dominated by NW-SE transmission lines rather than the expected east-west lines

Corresponding author: T. Divett, tim.divett@otago.ac.nz

Abstract

Transformers in New Zealand's South Island electrical transmission network have been impacted by geomagnetically induced currents (GIC) during geomagnetic storms. We explore the impact of GIC on this network by developing a thin-sheet conductance (TSC) model for the region, a geo-electric field model, and a GIC network model. (The TSC is comprised of a thin-sheet conductance map with underlying layered resistivity structure) Using modeling approaches that have been successfully used in the United Kingdom and Ireland, we applied a thin-sheet model to calculate the electric field as a function of magnetic field and ground conductance. We developed a TSC model based on magnetotelluric surveys, geology, and bathymetry, modified to account for offshore sediments. Using this representation, the thin-sheet model gave good agreement with measured impedance vectors. Driven by a spatially uniform magnetic field variation, the thin-sheet model results in electric fields dominated by the ocean-land boundary with effects due to the deep ocean and steep terrain. There is a strong tendency for the electric field to align northwest-southeast, irrespective of the direction of the magnetic field. Applying this electric field to a GIC network model, we show that modelled GIC are dominated by northwest-southeast transmission lines, rather than east-west lines usually assumed to dominate.

1 Introduction

The electrical transmission network in New Zealand's South Island has been impacted by Geomagnetically Induced Currents (GIC) during geomagnetic storms, for example in November 2001 [*Marshall et al.*, 2012; *Mac Manus et al.*, 2017]. GIC are induced in electrical transmission lines and other engineered structures during space weather events (or geomagnetic storms). At mid latitudes GIC often appear to be linked to the arrival of coronal mass ejections (CME). For an overview of the physical processes we suggest a relevant textbook (e.g., *Bothmer and Daglis* [2007]). During a CME, large quantities of high speed plasma are ejected from the Sun. When a CME hits the Earth's magnetosphere the plasma and associated change in magnetic field has an impact on the magnetosphere and ionosphere. This can strongly enhance the electrojet currents, which contribute to magnetic field variations at ground level. This magnetic field variation, coupled through the resistive earth and relatively conductive ocean in turn induces an electric field at ground level. While the induced electric field may only be in the order of a few mV/km, over the length of a transmission line the induced electromotive force along the transmission line can be significant. During strong geomagnetic storms this electromotive force can be strong enough to drive tens or hundreds of amps of quasi-DC GIC to local earth through a transformer connected to that transmission line.

Among space weather effects, GIC in power lines are potentially hazardous to economic activity with large social impacts. GIC cause damage to transformers located within substations connected by the long transmission lines which make up the national grid of most developed countries (*Bothmer and Daglis* [2007]). One of the most commonly discussed GIC events is the disruption to electrical transmission systems in Quebec, Canada during the March 1989 storm (*Boteler* [1994]; *Bolduc* [2002]). However, direct damage to transformers by spot heating or by longer term repeated heating of the insulation around transformers has also occurred in several low to mid geomagnetic latitude countries including the UK (*Erinmez et al.* [2002]), South Africa (*Gaunt and Coetzee* [2007]), Brazil (*Trivedi et al.* [2007], China (*Liu et al.* [2009]), Spain (*Torta et al.* [2012]) and Australia (*Marshall et al.* [2013]), as well as New Zealand.

The South Island of New Zealand is located at a similar geomagnetic latitude to the United Kingdom (UK). With a geomagnetic latitude of 53 ° South, Dunedin is at the same geomagnetic latitude as Edinburgh, and the same relative location within the island. It is not surprising therefore that the South Island's electrical transmission network has experienced similar impacts as that in the UK and that transformers at substations in Dunedin have been impacted by GIC.

Further, the island nature of both New Zealand and the UK makes the similarities even more compelling when faced with the task of modeling the geo-electric fields around New Zealand. The thin-sheet electromagnetic model developed by *Vasseur and Weidelt* [1977] (hereafter VW77) has been used successfully to model the electric field around the UK for GIC by *Mckay* [2003]. Because of the similarities (i.e.: geomagnetic latitude and island size) between the countries, VW77's model should be applicable to New Zealand with only modifications to the conductance model to account for New Zealand's geology and oceanography.

However, the continental shelf surrounding the UK is the largest in the world, with water depth less than 300 m, and the topography of the UK is relatively low lying (< 1400 m). In contrast New Zealand's rather deeper bathymetry (> 4500 m) and higher topography (> 3000 m) have more in common with Japan, the island nations of the East Indian Seas, Kamchatka, or the west coast of North and South America. The bathymetry affects the electric field due to the varying conductance of the top 10 km surface layer of the Earth. A deeper layer of conducting sea water on top of more resistive rock increases the total conductance of the surface layer compared to shallow sea water. Further, mountainous rock tends to be highly resistive compared to saturated sediments. Hence, while New Zealand's geomagnetic latitude is similar to the UK, the conductance of the upper crust and potentially the resulting induced electric fields are very different to the UK.

These induced electric fields can be used to calculate the current induced in an electrical transmission network through a network model. Previous GIC network models which calculate induced current at each node on an electrical network have often been based on one of two methods: the *Lehtinen and Pirjola* [1985] (hereafter LP85) matrix method or the Nodal Admittance Matrix method traditionally preferred by electrical engineers. *Boteler and Pirjola* [2014] present a description of both methods and show that the two are mathematically equivalent. The implementation of the matrix method by *Mckay* [2003] that was further developed by *Beggan et al.* [2013], *Kelly et al.* [2017], and *Blake et al.* [2016] has been successfully applied in GIC studies in the UK, Irish, and French networks. Recently *Richardson and Beggan* [2017] validated this GIC network model using the test network of *Horton et al.* [2012].

All of the previous GIC studies we have discussed so far are designed as hindcasting tools that can be used to estimate extreme events and compare mitigation tactics. There are other problems that a GIC model could be applied to, such as forecasting or nowcasting [*Bonner and Schultz*, 2017]. However, the present paper concentrates on the linked geo-electromagnetic and GIC network modeling that is required to develop a hindcasting tool.

In the current paper we have developed three models required to explore geo-electric fields around New Zealand and the GIC in the South Island's electrical transmission network. These are: 1) a thin-sheet conductance (TSC) model, 2) a model of the geo-electric fields, and 3) a GIC network model for the South Island's transmission network. We describe our modeling method in Section 2 with results of these models shown in Section 3. While the exact TSC model and the details of the transmission network are specific to New Zealand, the challenges involved in developing these models from available data should be applicable to the broader GIC research community. Further, the process of developing the TSC model from magnetotelluric soundings as well as geology and bathymetry may be of interest to GIC researchers in other countries, such as Japan, with deep ocean near the coast or a similar tectonic environment to New Zealand's.

2 Electric field and GIC modeling method

We have used a three stage modeling approach similar to that used successfully to calculate GIC in the United Kingdom and Ireland by *Mckay* [2003], *Thomson et al.* [2005], *Beg-*

gan et al. [2013], *Beggan* [2015], and *Blake et al.* [2016]. The first stage is the development and validation of a suitable TSC model for New Zealand and the surrounding oceans. This is based on magnetotelluric studies, geological maps, and bathymetry. We then calculated the ground level electric field induced by an idealized magnetic field over the spatially varying TSC model using the thin-sheet model of VW77. Finally, we used the electric field as the input to the GIC network model of New Zealand's high voltage electrical transmission network to calculate the GIC flowing through each substation in the network.

2.1 Conductance representation and validation of electric field model

Numerical modeling to calculate the surface electric field induced by a time varying magnetic field uses the thin-sheet technique of *Vasseur and Weidelt* [1977]. In this technique 3-dimensional variations in electrical conductivity are represented by 2-dimensional spatial variations in the conductance of a thin sheet at the surface of an underlying layered electric conductivity profile. Numerical considerations dictate that the technique is valid when the following two conditions are met:

$$\left(\frac{h}{\eta}\right)^2 \ll 1 \tag{1}$$

$$h \ll 1 \tag{2}$$

where h is the thickness of the thin-sheet and η is the skin-depth in the thin-sheet, both expressed in units of δ, the skin-depth in the underlying layered structure. Additionally the 2-dimensional spatial grid on which the conductance is defined must have a unit spacing of less than $\delta/4$. For a typical period of 10 minutes, $\delta = 190$ km so $h = 0.10$. In the South Island $\eta \geq 0.8$ in units of δ so $(h/\eta)^2 \leq 0.13$ and clearly the conditions in Equations 1 and 2 as well as the grid criteria are met.

A previous thin-sheet model of the New Zealand region was presented by *Chamalaun and McKnight* [1993] to represent geomagnetic induction arrow responses measured during a magnetometer array study covering both the North and South Islands of New Zealand. Their TSC model incorporated a representation of the surrounding bathymetry, with conductances ranging from 3300 to 16500 S, and used a uniform conductance of 0.1 S for land areas. *Pringle et al.* [2000] used a similar model to investigate the effect on induction arrows of a high conductance region associated with the Alpine Fault. However, New Zealand sits on the boundary between the Pacific and Australian tectonic plates and, resulting from the tectonic setting, significant conductivity variations exist across both the North and South Islands. Thus, development of a model of induced electric fields in New Zealand which can be used to assess the risk to the New Zealand power system from GIC flows requires a much more detailed on-land conductance model which satisfactorily represents these variations.

Within the North Island many magnetotelluric (MT) studies have been conducted to investigate the conductive structure associated with the Central Volcanic Region and Taupo Volcanic Zone [*Ingham*, 2005; *Heise et al.*, 2008, 2010, 2014; *Bertrand et al.*, 2012, 2013], the major volcanoes [*Cassidy et al.*, 2009; *Ingham et al.*, 2009; *Stagpoole et al.*, 2009], and the subduction interface along the east coast [*Ingham et al.*, 2001; *McLoughlin et al.*, 2002; *Heise et al.*, 2012]. Fewer such studies have been conducted within the South Island and, in general, have concentrated on elucidating the conductivity structure associated with the active uplift of the Southern Alps, and the Alpine Fault [*Ingham*, 1996, 1997; *Wannamaker et al.*, 2002, 2009]. The majority of these studies present conductivity structure in the form of 2-dimensional maps derived from MT measurements along individual transects of sites. In all such maps significant lateral variations in conductivity structure occur down to at least mid-crustal depths (20 to 40 km). To attempt to account for these variations the thin-sheet model that has been used in the current study considers a thin sheet, divided into 96 × 96

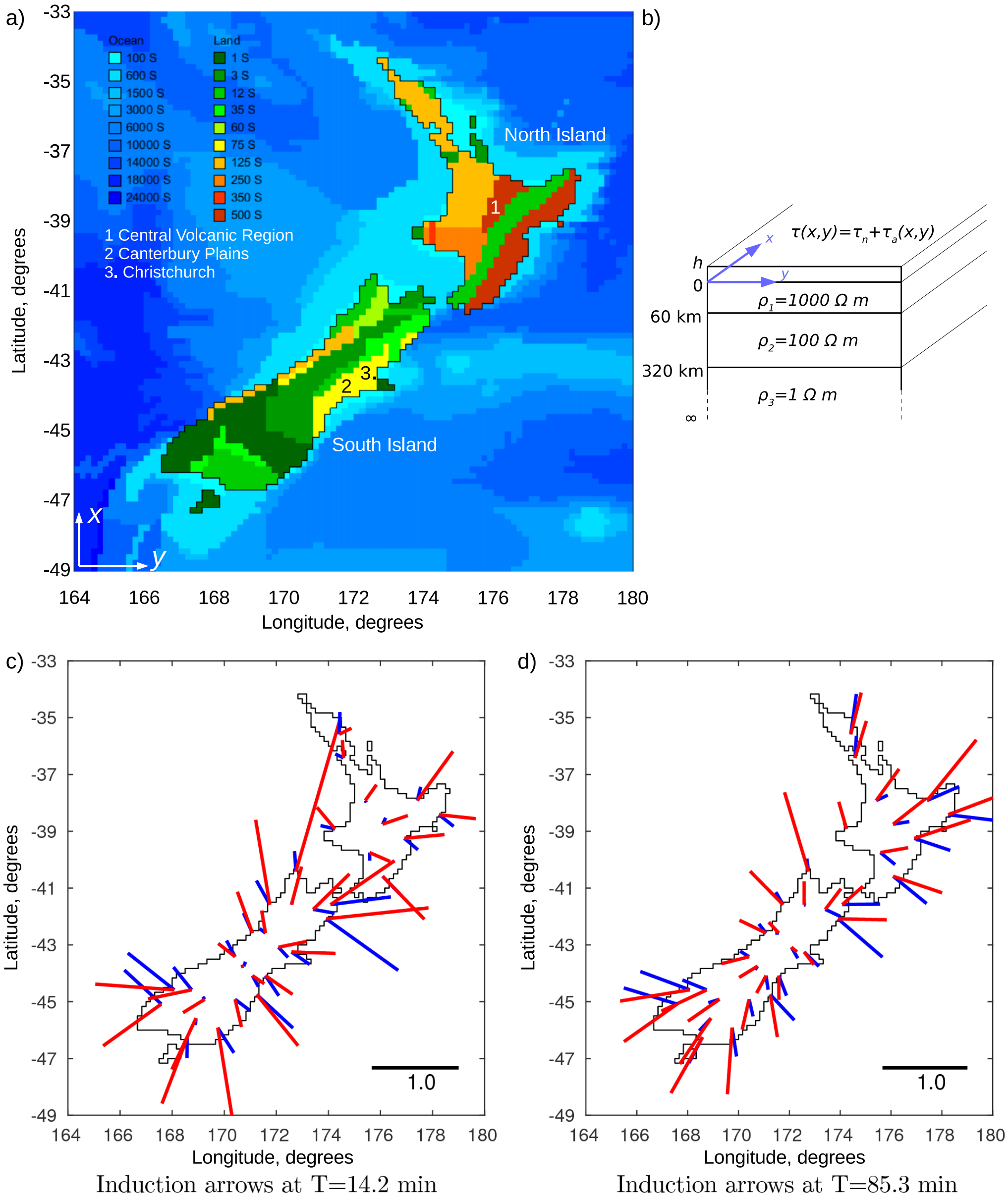

Figure 1. (a) Initial thin-sheet conductance map for New Zealand. Grid spacing is 1/6 degree (roughly 20 km). (b) Underlying layered resistivity structure. Together (a) and (b) comprise the *initial* thin-sheet conductance (TSC) model. Initial is in contrast to the *adjusted* thin-sheet conductance model shown later in Figure 3. (c) and (d) Comparison of calculated and measured real induction arrows at periods of variation of (c) 14.2 minutes and (d) 85.3 minutes. Model arrows, calculated using (a) and (b) as input to the thin-sheet model, are shown in blue. Measured arrows, from *Chamalaun and McKnight* [1993], are in red.

square cells (16 degrees North × 16 degrees West) with a grid spacing of 1/6 of a degree (roughly 20 km). We used this grid spacing to meet the thin-sheet model criteria that the length of a cell is less than $\delta/4$. The initial thin-sheet conductance model, comprising the thin-sheet conductance map and the underlying layered structure, is shown in Figure 1a and 1b. The on-land conductance of each cell represents the integrated conductance of the upper 20 km of the crust. The bathymetry and an assumed seawater conductivity of 3 Sm^{-1} are used to define the conductance of the surrounding ocean. The underlying layered structure consists of 3 layers, with resistivity of 1000, 100 and 1 Ωm and layer boundaries at 60 and 320 km depth. This allows the response to variations of the magnetic field with periods of 30 s upwards to be modeled without violating conditions 1 and 2 (Equations 1 and 2). The thin-sheet conductance is the total conductance $\tau = \tau_n + \tau_a$ composed of a background normal conductance (τ_n) and anomalous conductance (τ_a), as required for the thin-sheet model. The assumed normal conductance used in our thin-sheet model calculations is 24000 S, representative of the deep ocean surrounding the model domain.

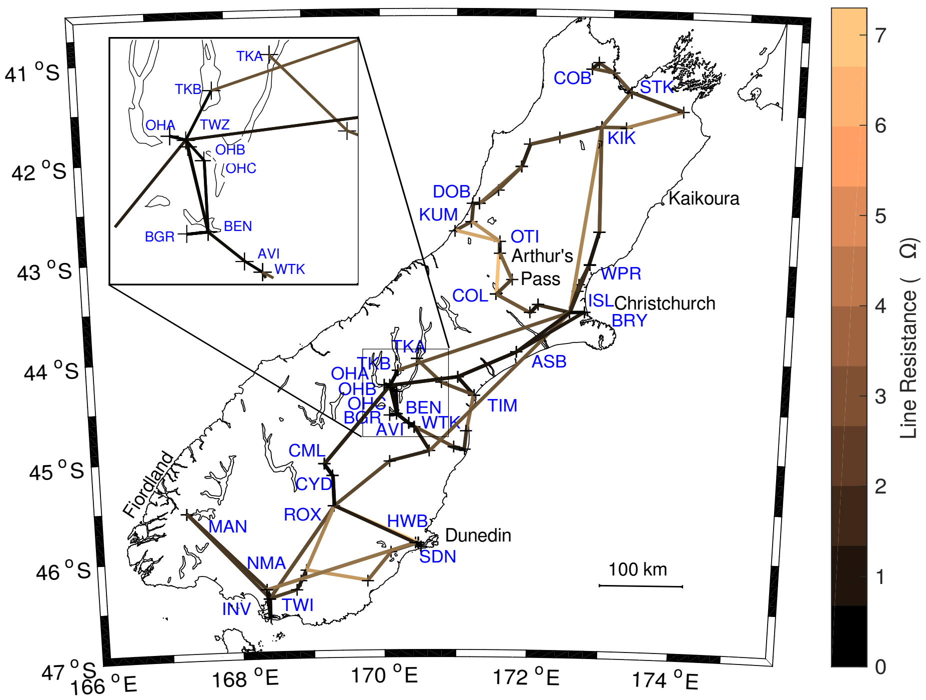

Figure 2. The South Island of New Zealand showing locations discussed in the text, transmission line resistance and substation node locations in the South Island network model.

On-land the most conductive features are in the North Island . These represent the conductive Tertiary sediments along the east coast and the volcanically active centre of the North Island. In general the conductance in the South Island is lower than in the North Island (Figure 1 a). Within the South Island, more conductive regions are the Canterbury Plains on the central-east coast around Christchurch (see Figure 2) and the sediments along the west coast of the South Island. These regions are adjoined by the narrow conductive zone associated with the Alpine Fault. The Alpine Fault runs up the spine of the South Island towards the western edge of the Southern Alps. Very low conductance is associated with the main ranges of the Southern Alps which run from southwest to northeast along the length of the South Island. However, an absence of field data means that the integrated conductance in the south of the South Island is essentially unknown and values south of a latitude of approximately 45 °S are based on surface geology.

Geomagnetic induction arrows (originally developed independently by *Parkinson* [1962] and *Wiese* [1962]) are calculated from frequency dependent complex transfer functions (T_x and T_y) relating variations in the vertical component of the magnetic field to those in the horizontal field $B_z = T_x B_x + T_y B_y$. Real and imaginary induction arrows are then calculated from the transfer functions as having magnitudes

$$|R| = \sqrt{T^2_{x\,real} + T^2_{y\,real}} \tag{3}$$

$$|I| = \sqrt{T^2_{x\,imag} + T^2_{y\,imag}} \tag{4}$$

and directions

$$\phi_R = atan(T_{y\,real}/T_{x\,real}) \tag{5}$$

$$\phi_I = atan(T_{y\,imag}/T_{x\,imag}) \tag{6}$$

In the Parkinson convention the direction of the real arrow is reversed so that it points towards regions of high electrical conductivity, with a magnitude which becomes smaller the greater the distance from the conductivity boundary. Although the behavior of imaginary arrows is more complicated, maps of induction arrows at different periods across a region have long been used in electromagnetic induction studies as a visual representation of the location of conductivity anomalies.

Following their magnetometer array study covering New Zealand *Chamalaun and McKnight* [1993] listed real and imaginary induction arrows at two periods of magnetic variation (14.2 and 85.3 minutes). As a means of providing some validation of the thin-sheet conductance model we have compared the real induction arrows with the arrows we calculated from the thin-sheet model (Figure 1c and 1d respectively). These modelled arrows were calculated using the thin-sheet conductance map, and layered resistivity structure shown in Figure 1a and 1b respectively.

The directions of real induction arrows are significantly affected by the discretization of the coast. Nevertheless it is clear that at both periods the size of the model induction vectors given by the thin-sheet model significantly underestimate the measured arrows at several sites. This is particularly noticeable in the south-east and north-west of the South Island and, for 14.2 minutes period, also along the east coast of the North Island.

In their TSC model, *Chamalaun and McKnight* [1993] had two features which differ significantly from our representation, shown in Figure 1. Firstly, they used a minimum ocean conductance of 3300 S which significantly increases the contrast between land and ocean compared to a thin-sheet model showing the true bathymetry where the minimum conductance close to the land is generally < 500 S. Secondly, compared to the uniform resistivity of 1000 Ωm down to 60 km depth used in the resistivity structure of Figure 1b, their underlying layered resistivity structure used a value of 10000 Ωm between depths of 10 and 60 km and a value of 1000 Ωm from 60 to 80 km.

It can be argued that the small ocean conductances shown in Figure 1a for the near-land regions are in fact unrealistic as they do not take into account the underlying sediment on the sea floor which is also likely to be conductive. Indeed, updated maps of ocean sediment thickness [*Whittaker et al.*, 2013], based largely on velocity-depth functions from sonobuoy/refraction velocity solutions, suggest that sediment thickness around New Zealand

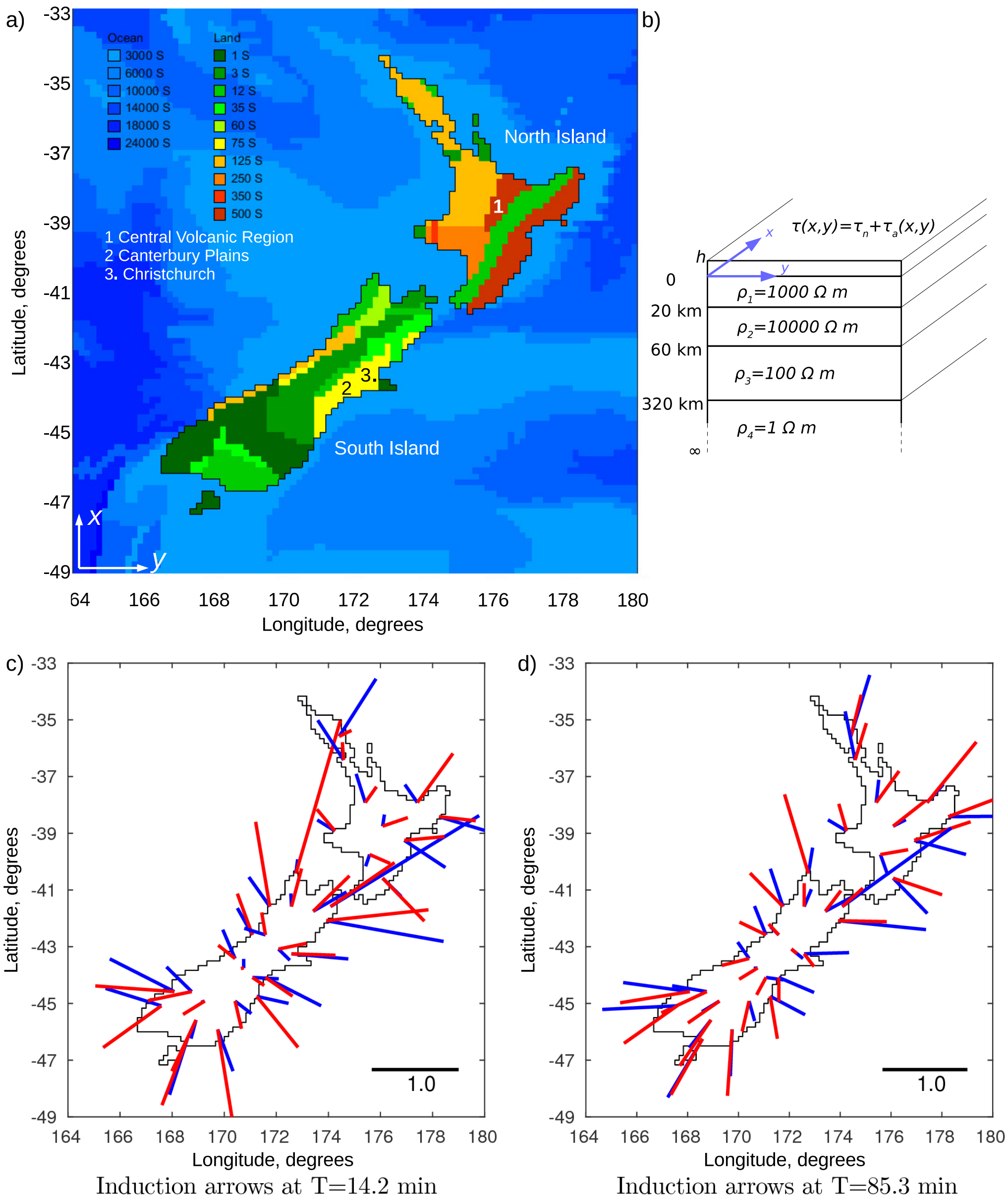

Figure 3. (a) and (b) comprise the *adjusted* thin-sheet conductance (TSC) model for New Zealand, comprised of the conductance map (a) and underlying layered resistivity structure (b). Grid spacing is 1/6 degree (roughly 20 km). (c) and (d) Comparison of calculated and measured real induction arrows at periods of variation of (c) 14.2 minutes and (d) 85.3 minutes following refinement of the conductance and layered resistivity inputs to the thin-sheet model as discussed in the text. Model arrows are shown in blue, measured arrows in red.

is around 1000 m. Allowing for saline water circulation in at least the upper part of such sediments it appears reasonable to follow Chamalaun & McKnight and use a minimum ocean conductance of 3000 S. When this is done the match between the lengths of model and measured arrows improves in many places (Figure 3c and 3d), especially along the east coast of the South Island. However, at other locations the calculated arrows remain significantly smaller than the measured arrows.

The fit of model arrows with the field arrows is further improved by using a layered resistivity structure which has a resistivity of 10000 Ωm between 20 and 60 km depth. The result of the combination of improvements is shown in Figure 3c and 3d. The length of the model arrows gives a good match to the field arrows everywhere except in the extreme north-west of the South Island and along the Central Volcanic Region in the centre of the North Island. However, the extremely large field arrows at the north-west tip of the South Island probably reflect features of the coastline which are too fine in detail to be incorporated in the thin-sheet model.

The method we have used to model electric fields was adapted to model surface electric fields for GIC studies, originally by [*Mckay*, 2003]. Three dimensional electromagnetic models have been developed to calculate the electric field at the Earth's surface using integral methods [*Kuvshinov*, 2008; *Püthe and Kuvshinov*, 2013; *Püthe et al.*, 2014] or finite difference methods [*Mackie et al.*, 1994; *Uyeshima and Schultz*, 2000]). In the South Island in particular MT results are relatively sparse and have been concentrated on long cross-island profiles. In the North Island, where there have been many more MT sites, the conductivity structure is more complex resulting from the fact that New Zealand is tectonically active. However, neither of these factors invalidates the thin-sheet model. All the necessary conditions for validity are met in the period range of variations to which we have applied the thin-sheet model. Additionally, particularly in the South Island, away from MT sites a full 3-D model would still require input from a conductance model based on geology. It is not clear, therefore, whether a 3-D modelling approach would provide further predictive power to the understanding of GIC in New Zealand beyond that provided by the thin-sheet modelling approach.

In conclusion the TSC model, consisting of the conductance map and layered resistivity structure shown in Figure 3, does a reasonably good job of reproducing the measured real induction arrows, thus lending confidence to the validity of the conductivity representation for use in prediction of GIC.

2.2 Induced electric fields

In the thin-sheet model, GIC are assumed to be driven by the horizontal electric fields that are induced at the surface of the Earth by the temporal variation in horizontal components (northward and eastward) of the linearly polarized magnetic field. The electric field induced by the magnetic field is an elliptically polarized plane wave traveling normal to the Earth's surface in the direction of increasing depth ($+z$) such that the tip of the instantaneous wave vector traces out an elliptical helix in space and time given

$$E_x(t) = E_{0x} e^{-i(\omega t - \alpha_x)} \tag{7}$$

$$E_y(t) = E_{0y} e^{-i(\omega t - \alpha_y)} \tag{8}$$

where E_{0x} and E_{0y} are the complex field amplitudes in the x and y directions, respectively and α_x and α_y are the phases of these fields relative to the inducing magnetic field. The real components of equations 7 and 8 can be rearranged to the standard form of an el-

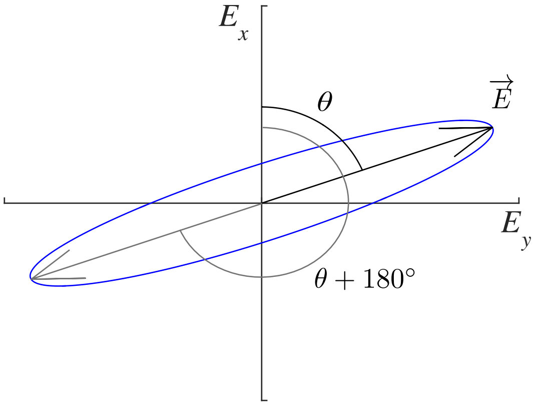

Figure 4. The elliptical trajectory of the tip of the time varying vector (blue), the semi-major axis used to represent the maximum value of $\vec{E}$ and the other semi-major axis (grey). θ, clockwise from North, is calculated using Equation 9.

lipse with semi-major axis inclined at an angle

$$\theta = \frac{1}{2} tan^{-1}\left(\frac{2cos(\alpha_y - \alpha_x)}{\frac{|E_x|}{|E_y|} - \frac{|E_y|}{|E_x|}}\right) \tag{9}$$

clockwise from north.An example of such an ellipse, with the direction of the semi-major axis and θ indicated is shown in Figure 4. Given that the maximum amplitude of the electric field is in the direction of the semi-major axis, θ, we use this direction for the input electric field to the GIC network model. Due to the symmetry of the ellipses there is also a maximum at $\theta + 180°$ and the decision to use θ or $\theta + 180°$ is based on consistency with the field direction in the deep ocean in the south westernmost cell of the domain. This directional ambiguity is irrelevant from the perspective of an oscillating electric field. However it is important to use a consistent reference direction when summing an electric field along a transmission line, as we will describe in Section 2.3. When calculating the current source in a transmission line due to the surface electric field, reversing the direction of E over neighboring cells purely due to this symmetry would result in near zero voltage. In contrast in a calculation undertaken with a consistent reference direction and the assumption that the electric field direction varies smoothly over neighboring cells, the electric fields add cumulatively along the path of a transmission line, as expected.

2.3 GIC network model of the South Island

The South Island is an ideal test case for GIC modeling because it is geographically isolated, electrically isolated, and while it is relatively small it contains many of the modern electrical engineering devices that are found in larger, less isolated networks. Further, the network is largely owned and operated by a single network operator, Transpower New Zealand Ltd. Although small parts of the network on the west coast of the South Island and in Tasman (north west of the South Island) are owned by other companies, Transpower maintains records of the network characteristics for these regions. The network is constantly changing with repairs and upgrades being made. For the present study all of the transmission line resistances, substation locations and earthing resistances have been supplied by Transpower, representing a snapshot of the network as it existed in late 2015.

The South Island high-voltage transmission network consists of transmission lines with three different voltage ranges: 50 or 66 kV, 110 kV and 220 kV. This network is only connected to the North Island by a High Voltage DC (HVDC) link. The South Island network is therefore effectively an isolated network of 64 nodes connected by 121 transmission lines.

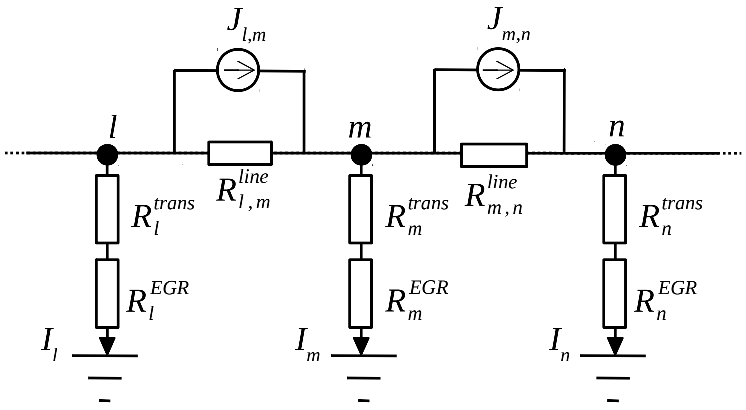

Figure 5. The node and connector representation that we use for New Zealand's high voltage transmission network, adapted from *Lehtinen and Pirjola* [1985] and *Beggan et al.* [2013].

Following the approach of LP85 we have represented the South Island network by substation nodes connected by line resistors and earthed through earth ground resistors as shown in Figure 5. The n^{th} element of the vector of perfect earth currents, $\overrightarrow{J} = [J_1 ... J_{121}]$, is the current that would flow to ground through a perfect earth connection (resistance to ground = 0) at the n^{th} substation. $\overrightarrow{J}$ can also be viewed as a current source applied over the impedance of the transmission lines that connects nodes [*Boteler and Pirjola*, 2014] as shown in Figure 5. $\overrightarrow{J}$ is calculated for each transmission line from the electric field, $\overrightarrow{E}$, along each transmission line with line elements $\overrightarrow{ds}$ using

$$J_n = \int \overrightarrow{E} \cdot \overrightarrow{ds}. \tag{10}$$

The GIC flowing to ground through each substation is calculated from the network admittance matrix, Y, and an earthing impedance matrix, Z, using

$$I_{GIC} = (1 - YZ)^{-1} J \tag{11}$$

following LP85. GIC varies slowly compared to the 50 Hz AC power so we assume that a DC treatment is sufficient and Y and Z are therefore assumed to be real. We note that the network inductance can be high so some lag could be introduced which we are not representing.

The earthing impedance matrix is built from the DC resistance of a single phase of the transformers at each substation, where we assume that the resistance of each substation is $R_n^{trans} = 0.5\,\Omega$ following a common approach used successfully in GIC models of European networks [*Beggan et al.*, 2013; *Blake et al.*, 2016; *Kelly et al.*, 2017]. This may be a little low for New Zealand's substations but facilitates a simpler comparison with previous modelling studies which have used this assumption. Transmission lines are assumed to be a single straight line between nodes. DC line resistance, R_{line}, represents the resistance to a DC current flowing in parallel in all 3 phases of a transmission line as supplied by Transpower NZ Ltd. R_{line} varies from $0.039\,\Omega$ for the 220kV line between Ohau B (OHB) and Twizel (TWZ), to $7.1\,\Omega$ for the 66kV line over Arthur's Pass between Coleridge (COL) and Otira (OTI) (locations shown in Figure 2). The resistances for parallel transmission lines connecting the same substations were added in parallel when building the network impedance matrix. We have assumed that the current through each of the 3 phases of transformers and transmission lines is the same and we only modelled one of the phases. This assumption is common in the GIC modeling community, as discussed by, for example *Boteler and Pirjola* [1998, 2017]; *Lehtinen and Pirjola* [1985]; *Pulkkinen* [2015].

In the LP85 matrix method each node is assumed to be earthed through an earth ground resistor (R^{EGR}). Earth Ground Resistance (EGR) is the resistance between the earth mat at a substation and a remote ground. Transpower regularly measure the EGR at each substation and, for this network model, have provided the most recent measurement available for each substation. The value of this resistance at different substations can be as different as an order of magnitude depending on a range of factors including local soil type, underlying rock conductance, soil moisture content, and earth grid size. EGR ranges from 0.04 Ω at South Dunedin (SDN), to 4 Ω at Kumara (KUM), with a mean of 0.63 Ω. A lower EGR resistance means that there is less impedance for GIC to enter the network at that location. Several substations do not have an earth connection on the high voltage side of the transformer because they use delta-Y transformers, where any earth connection is only on the low (local distribution) voltage side. Of the 63 substations on the high voltage transmission network only 28 are earthed on the high voltage side. GIC only flows to ground through the nodes that are earthed on the high voltage side. The unearthed substations are included in the network model to allow for branching of the network at those nodes. Further, keeping these unearthed nodes in the model means that the transmission lines pass through the unearthed node location which is more realistic than simply taking the most direct path between earthed substations.

We assume that the EGR is infinite at unearthed nodes. However, due to the matrix representation, using a truly infinite resistance results in a poorly scaled matrix inversion. Therefore, following *Boteler and Pirjola* [2017], to avoid dividing by zero during the matrix inversion these unearthed nodes have $R_{EGR} = 10^{10}\,\Omega$. This is a realistic but very large resistance compared with other resistances in the network model and avoids introducing the numerical roundoff errors that would occur as calculations of $I = V/R_{EGR} \to 0$ as $R_{EGR} \to \infty$.

3 Results

In this section we show results of driving the thin-sheet model of VW77 with the TSC model in Figure 3a and 3b. We applied a horizontal magnetic field variation of period $T = 600$ s, with a uniform direction (β), and magnitude ($|B| = 500$ nT) everywhere in the domain. β is measured in degrees clockwise from north. The direction of the magnetic field is varied in 10° increments from 0 to 350° to test the response of the electric field around New Zealand to magnetic field variations in varying direction and to test the susceptibility of the transmission network to these different directions. The resulting electric field for representative directions of the magnetic field shows features associated with the 2D surface conductance (Figure 6a to 6d for $\beta = 20$, 50, 120 and 140° respectively). The electric field directions shown in Figure 6 are the direction of maximum field magnitude in each cell as given by equation 9. The variation in electric field as β changes from 0 to 360° at a point representative of the Southern Alps is shown in Figure 7. The GIC caused by that electric field and the network topography is shown in Figure 8. When the magnetic field is oriented parallel with the main southwest to northeast axis of New Zealand's mountain backbone, spanning both islands, it results in the strongest electric fields and hence the highest GIC, relative to magnetic fields in other directions. The directions of these magnetic fields are $\beta = 20$ to 60° (in Figure 6a and 6b as well as Figure 8a and 8b) or 200 to 240°. Results for $\beta > 180°$ are not shown as they repeat the electric field and GIC in Figures 6 and 8 with directions rotated by 180°.

3.1 Modeled electric field around New Zealand

The strongest contrasts in the electric fields shown in Figure 6 occur at the coastline where weak electric fields in the highly conductive ocean and the strong electric fields on the

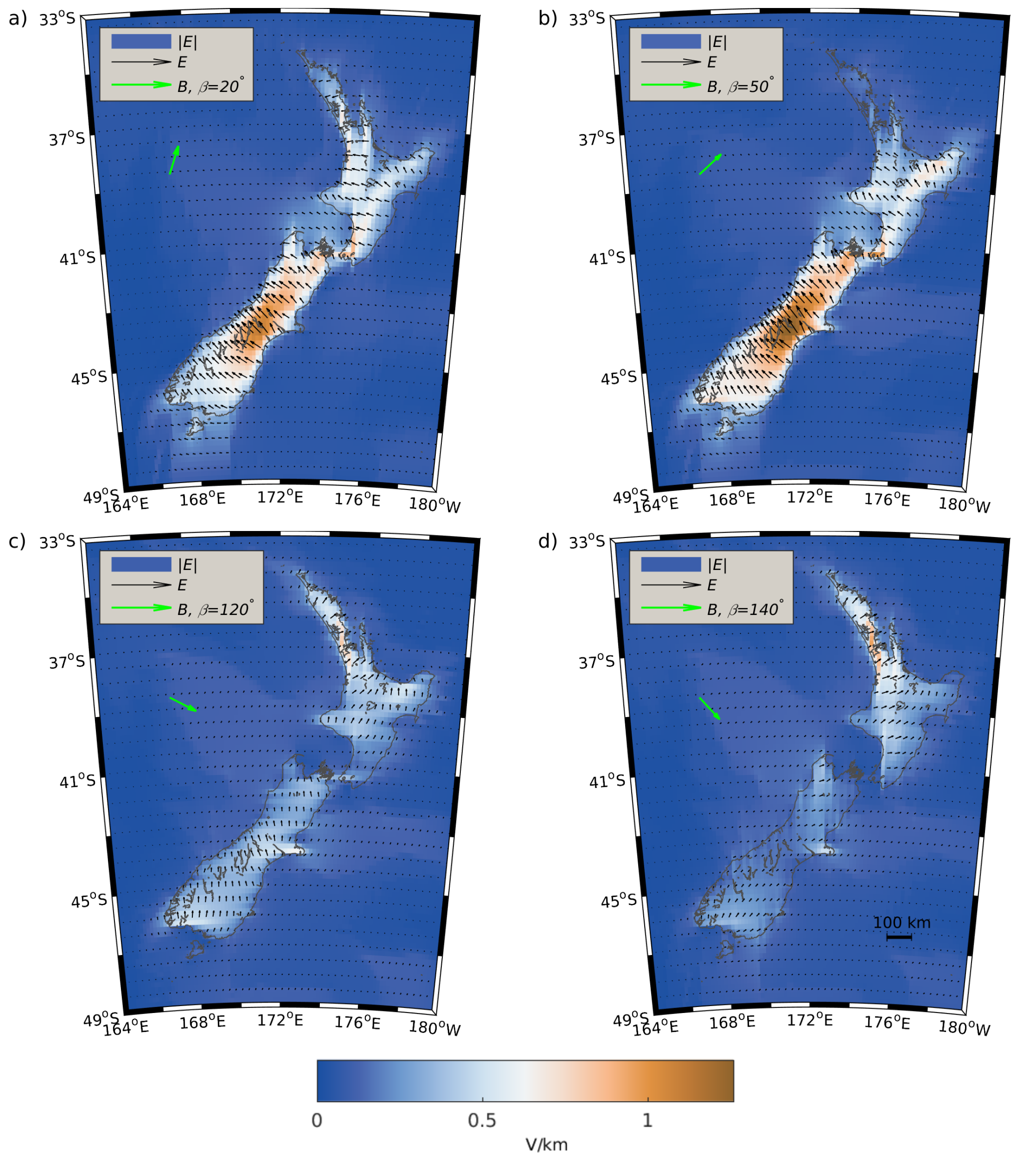

Figure 6. Electric fields calculated using the thin-sheet model driven by a uniform magnetic field variation with magnitude $|B| = 500nT$ and direction $\beta = 20, 50, 120$ and $140°$ in a) to d) respectively using the adjusted conductance representation in Figure 3). Magnetic field direction, clockwise from north, is indicated by the green arrow. Electric field directions are the direction of maximum field magnitude in each cell, as given by equation 9.

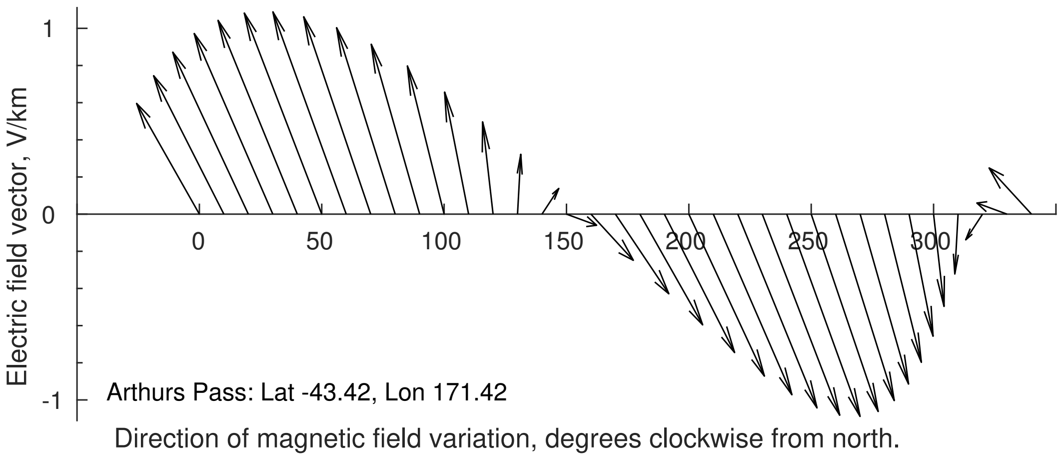

Figure 7. Representative electric field vector showing change in magnitude and direction at Arthurs Pass as the direction of the magnetic field changes relative to geographic north.

resistive land meet. The direction of the electric field in the deep ocean is predominantly 90 ° anticlockwise from the magnetic field direction. The strongest deviations in the on-land electric field away from 90 ° behind the magnetic field also occur at the coast where the electric field takes a direction perpendicular to the modeled coastline. (It should be noted that the discretization of the coastline represented in the thin-sheet model is shown in Figure 3a. This coarse coastline is representative of the line between cells on land and cells in the ocean as opposed to the geographical coastline shown in Figure 6.) Further, the largest induced electric fields occur in the highly resistive mountainous regions of the Southern Alps.

New Zealand's topography and bathymetry provide some small regions of especially high conductance gradient at the coast. The most notable regions where deep water with steep gradients occur near the coast are the 4.5 km deep water only 5 km, or a quarter of a grid cell, west of Fiordland (locations are indicated in Figure 2) and the 2 km deep Kaikoura Canyons rising steeply to the coast at Kaikoura. The high conductance of the deep seawater in the New Zealand region stretches the assumptions made by the thin-sheet model but as noted in Section 2.1 we have taken care to ensure that the assumptions about skin depth, grid size, and water depth are met. Furthermore many of the Fiordland fiords are too narrow to be resolved in the 20 km grid cells for this model of the New Zealand region. The effect of the fiords is probably small compared to that due to the steep coastal conductance gradient but would be worth exploring further with a higher resolution model around Fiordland, near Manapouri (MAN). However, this further work would require more detailed measurements of the ground conductivity in this region than are currently available.

Similar to the effect on the electric field near the coastline, offshore bathymetry features are highlighted by the electric field at regions of steep changes in bathymetry with associated steep conductance gradients, as seen in Figure 6. There is an increase in the electric field magnitude around offshore features such as Chatham Rise (east of Christchurch) and along the Hikurangi Margin (east of the North Island) where the thin-sheet conductance decreases sharply from 12000 S in 4000 m deep water to 3000 S in shallow water within a few grid cells. As well as the increased magnitude of the electric field, the direction is deflected from 90 ° behind the magnetic field towards the region of lower conductance in these offshore regions, in the same way as occurs at the coast. This effect also occurs south west of the South Island where an underwater ridge extends to the south west. Here there is a region of stronger electric fields relative to the deeper ocean surrounding it. These local increases in electric field in relatively shallow offshore water will not affect GIC in the land based transmission network, but are an interesting aspect of the modeled electric field.

Figure 7 shows how the magnitude and direction of the electric field at a representative point near Arthurs Pass varies with the direction of the inducing magnetic field variation. The direction of the electric field at this location is representative of the strong electric field over most of the South Island's mountainous region. Interestingly, over the majority of the South Island there is very little change in the direction of the electric field as the direction of the imposed magnetic field rotates from 350 ° to 120 ° (Figure 6 and Figure 7). Over this range of magnetic field directions the direction of the maximum induced electric field over the majority of the South Island varies only a few degrees away from northwest. As the magnetic field direction continues to rotate clockwise from 120 ° (Figure 6c) to 170 ° the direction of the electric field changes quickly by 180 ° while the magnitude of the electric field remains small.

This strong dominance towards a northwest orientation of the electric field over the majority of the country shows that the shape of the island has more of an effect on the direction of the electric field than the direction of the inducing magnetic field. However, the magnitude of the electric field changes considerably as the direction of the magnetic field changes from 350 ° to 120 °. While the strongest electric field occurs when the driving magnetic field is oriented parallel to the main axis of the islands ($\beta = 50\,^\circ$), the electric field is weakest over the majority of the country when the magnetic field is perpendicular to the island's main axis ($\beta = 140\,^\circ$), as shown in Figure 6d. $|E|$ is within 10% of the maximum for magnetic fields from 20 °to 80 ° and then drops smoothly as the magnetic field direction increases from 80 ° to 140 °. The exception to this is the Northland peninsula, extending from the northern tip of the North Island to the main part of the North Island, which is oriented perpendicular to the main axis of the country. In this region these patterns are reversed due to this perpendicular orientation; $|E|$ is strongest for $\beta = 140\,^\circ$ and weakest for $\beta = 50\,^\circ$. These trends are mirrored for magnetic fields in the opposite direction, with the direction of the electric field also reversing.

If we assume that the magnetic field is induced by the auroral electrojet with an equivalent current that is aligned to geomagnetic west then the strongest magnetic field during a real geomagnetic storm would be aligned to geomagnetic north. From the north to the south of New Zealand geomagnetic north varies between 18 ° and 26 ° clockwise of geographic north [*Gns.cri.nz*, 2015]. This is at most 30 ° from the direction which causes the strongest electric fields. A magnetic field in this direction induces an electric field within 10% of the maximum electric field strength. So the long, thin shape of New Zealand's main islands and the orientation of the main axis close to geomagnetic north combine to enhance the effect of the induced electric field in New Zealand.

3.2 GIC induced by the electric field around New Zealand

The GIC calculated using the substation level network model of the South Island's power transmission network is shown in Figure 8a to 8d for an inducing magnetic field with direction $\beta = 20$, 40, 120 and 140 °, respectively. For each substation the total current flowing to ground is indicated by circle size on the map and by the bar chart to the right of each map. GIC in Figure 8a to 8d have been calculated using the electric fields shown in Figure 6a to 6d respectively. As expected, the highest currents occur when the driving magnetic field is nearly parallel to the orientation of the island, that is $\beta = 20$ and 50 °. The strongest electric field results in slightly stronger GIC at all substations for $\beta = 50\,^\circ$ compared with 20 °. In general the weakest GIC flows occur when the inducing magnetic field is perpendicular to the South Island, i.e.: at $\beta = 120$ and 140 °. Thus the GIC response of the network is greatest for a magnetic field variation oriented with geomagnetic north ($\beta = 23.5\,^\circ$ in the middle of the South Island). This is the direction of induced magnetic field that we would expect due to an east-west auroral electrojet and shows that the orientation of the South Island does indeed have a strong impact on the GIC magnitude flowing in the South Island electrical transmission network.

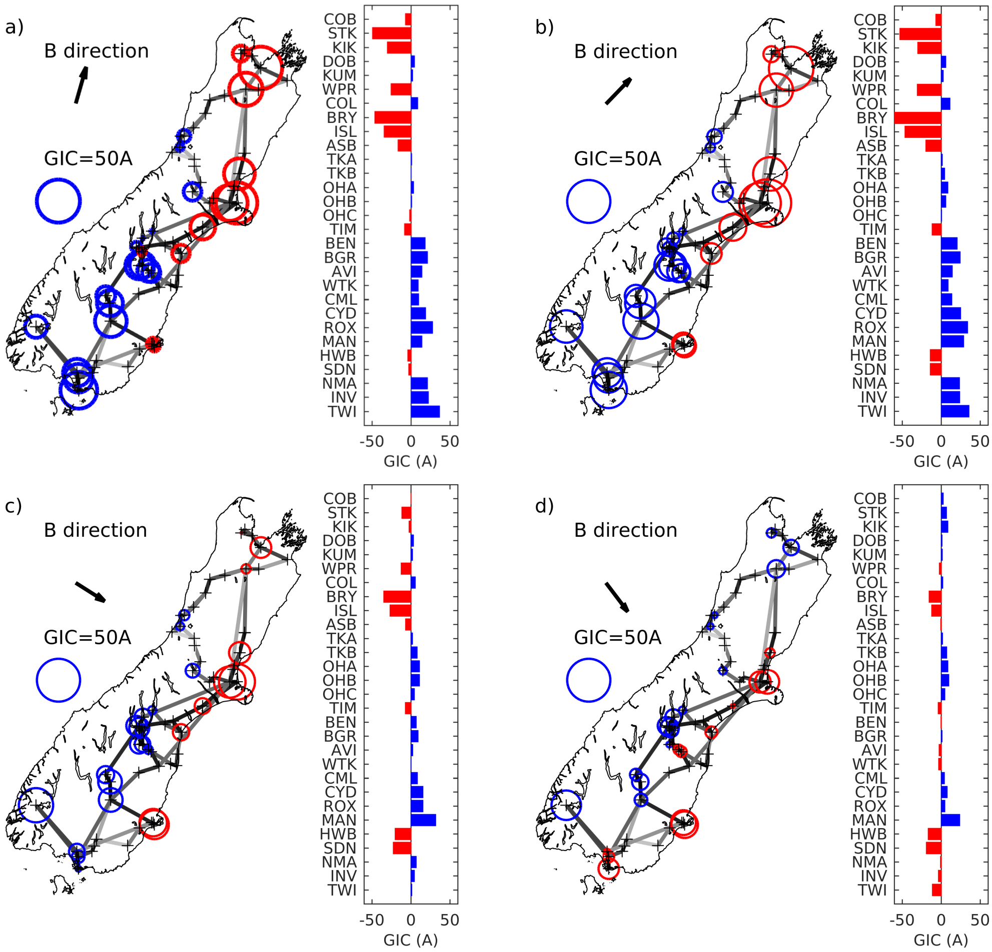

Figure 8. GIC at earthed substations in the South Island for magnetic field direction $\beta = 20, 50, 120$ and $140\,^\circ$ in panels a to d due to the electric fields in Figure 6. GIC, calculated using Equation 11, flowing to ground at each substation (given in Figure 2) is shown by circle size on the map (blue positive, red negative) and as a bar for each substation from south (bottom) to north (top).

The most striking feature of the calculated GIC distribution is the high spatial variability in the GIC magnitude and the small number of substations that experience high GIC. For instance when $\beta = 50^\circ$ only STK, BRY and TWI have GIC greater than 40 A. In contrast, we calculated GIC of less than 5 A at 10 of the 29 earthed substations. The high GIC at BRY, ISL and STK substations are particularly enhanced by the path of transmission lines passing through the high electric fields in the mountainous Southern Alps. Any transmission line that crosses these regions of high electric field strength will have a high electromotive force between earthed substations at each end of the line, leading to the high GIC shown at these substations. However more resistive transmission lines, such as the 66kV line over Arthur's Pass between COL and KUM, result in much smaller GIC at those substations, despite traversing the region of high electric field.

The other spatial pattern revealed by our modeling of GIC across the South Island is the difference between positive current in the south and west compared to negative current in the north and east. This represents current flowing into the transmission network on one side of the country and from the network to ground on the other side of the country. The direction of the flow is not important to transformers at each substation. They will be equally affected by a current flowing in either direction, and the actual direction is largely irrelevant due to the oscillating nature and elliptical polarisation of the electric field. Thus, although it shows an interesting effect of GIC in the network, the direction of the current does not make a difference to the potential impact on transformers. The direction of this trend flips by 180° for imposed magnetic field directions greater than 140°. In fact the start of this change can be seen in Figure 8d where the GIC in the south (TWI and INV) which were positive for $\beta = 120^\circ$ are negative for $\beta = 140^\circ$ and vice versa for KIK and STK in the north.

The effect of New Zealand's especially high coastal conductance gradients and associated electric fields in Fiordland and Kaikoura (discussed in Section 3.1) on modelled GIC is probably fairly small due to the network topography around these locations, except around Manapouri (MAN in Figure 2). The only high voltage transmission lines near the high conductance gradients at Kaikoura are the HVDC link. This line is essentially isolated from the rest of the network for the purpose of GIC by thyristor converters connecting it to the rest of the network. As a result the impact of the Kaikoura Canyons on modeled GIC is probably minimal. The other region with high coastal conductance gradients is Fiordland. The nearest transmission line connects Manapouri (MAN) to Invercargill (INV). This line starts ~ 50 km inland from the ocean and the strongest nearby electric fields are west of the substation. The transmission line runs parallel to the electric field which is perpendicular to the coastline. Therefore the effect of strong coastal conductance gradients and associated strong electric fields helps to explain why the modeled GIC is relatively high at the Manapouri substation.

4 Discussion

The strong tendency for electric fields to orient northwest to southeast is due to the shape and geographic orientation of New Zealand. This contributes to a high potential for GIC over the majority of the country, but especially the South Island. Further, due to this effect the highest GIC should be induced in lines oriented northwest-southeast, supported by the GIC in Figure 8. This contrasts with the commonly held maxim that the strongest GIC will be induced in lines that run in the east-west direction [*Crane*, 1990; *Gorman*, 2012]. In free space a northward magnetic field will induce an eastward electric field. This approximation may hold reasonably well in a large continent, but does not hold true for the long, thin islands of New Zealand. It is likely that this orientation of maximum electric field direction would also hold true for other long, thin islands or peninsulas that have a main axis that is not oriented north-south (for example Japan, Borneo, Java, Vancouver Island (British Columbia, Canada) or the Kamchatka peninsula).

There is however, a competing effect due to the dominant directionality of transmission lines in an island or continent. The South Island does not have very long east-west lines compared to the north-south line length. In the UK and Ireland, on the otherhand, there are long east-west lines. These long UK and Irish lines tend to show large GIC when the northward component of the magnetic field becomes dominant during big geomagnetic storms and in 1 V/km standard modelling tests [*Beggan et al.*, 2013; *Blake et al.*, 2016]. Further, in Europe, and North America long east-west transmission lines probably play a factor in compensating for any other important direction of the electrojet (other than east-west). This compensation is probably due to the simple fact that the longest lines provide the longest path for the accumulation of the electromotive force and hence current source (J_n in equation 10).

The deflection of the electric field towards a direction perpendicular to the coastline is consistent with the geomagnetic coast effect (*Parkinson and Jones* [1979]; *Mckay and Whaler* [2006]). This tendency for the direction of the coastline to dominate the direction of the modelled electric field is likely to have the strongest effect on GIC in coastal transmission lines oriented perpendicular to the coast. As such, in New Zealand, those substations at Invercargill (INV), Tiwai (TWI), Dunedin (HWB, SDN and TMH) and Christchurch (ISL and BRY) which are connected to transmission lines oriented perpendicular to the coast are probably the most affected by this coastal phenomenon. This is one factor which contributes to the high spatial variability of the modelled GIC.

Further, this high spatial variability matches observations of GIC in New Zealand reported by *Marshall et al.* [2012] and *Mac Manus et al.* [2017]. The strongest modeled GIC are at substations near the coast confirming that location of the substation within the network plays an important role in the distribution of GIC. This matches the findings of *Beggan et al.* [2013] that GIC are especially high at substations near the ends of coastal peninsulas in the United Kingdom. Further, our finding that GIC flows into the transmission network through southwestern substations and out through those in the northeast in New Zealand also matches a similar trend found by *Beggan et al.* [2013] for GIC in the United Kingdom. This confirms that the obvious geographic similarities between New Zealand and the United Kingdom do indeed transfer to modelled GIC. Direct comparison between the modeled GIC flow in the present work and the transformer level GIC observations reported by *Marshall et al.* [2012] and *Mac Manus et al.* [2017] would require a transformer level network model rather than the substation level network model that we presented in the current paper. A transformer level network model is a network model in which each individual transformer at each substation is represented by the specific DC characteristics for that transformer.

The modeled GIC in Figure 8 is the total GIC flowing to earth at each substation. Some substations have considerably more transformers than others. For example HWB has only two auto-transformers in parallel between the 220 kV bus, the 110 kV bus and the earth grid. On the other hand ISL has 3 normal transformers between the 220 kV bus and the 66 kV bus as well as 3 normal transformers converting the 220 kV to low voltage for local distribution. STK is even more complicated. We have assumed that all of the transformers at each of these substations can be represented by a single 0.5 Ω resistance, following *Beggan et al.* [2013] and *Kelly et al.* [2017]. Varying resistance of each transformer, different electrical configuration of normal transformers, auto transformers or different voltage levels have not, as yet, been represented in the network model. Adding this level of detail to the network model, as well as driving the thin-sheet model with a spatially varying magnetic field which is more representative of a space weather storm, may improve the match between modeled and observed GIC. Developing these further aspects of the model is the focus of ongoing work.

5 Conclusions

In this study we have developed a three-stage GIC modeling approach for New Zealand's South Island electrical transmission network based on the methods developed for the United Kingdom, Ireland, and France. We started by developing a new 2D 20 km × 20 km grid, surface conductance map, and an underlying layered half space resistivity depth profile. We used this TSC model and a spatially uniform magnetic field to drive VW77's thin-sheet electric field model in order to calculate the electric field around the New Zealand region. We validated the thin-sheet model and the conduction representation of New Zealand by comparing modeled induction vectors with those observed by *Chamalaun and McKnight* [1993]. This showed that the initial TSC model, which was based on a combination of compiled magnetotelluric observations and geology, needed to be refined to account for highly conductive sediment offshore as well as modifying the resistivity depth structure. This adjusted TSC model yielded induction vectors that were in good agreement with inductance vectors presented by *Chamalaun and McKnight* [1993], as discussed in Section 2.1 with reference to Figure 3c and 3d.

We used the electric fields generated by the thin-sheet model, assuming a monochromatic plane wave with a 600 s period, as the input to a substation level GIC network model describing the electrical transmission network in New Zealand's South Island. This approach was again based on those previously applied successfully in the United Kingdom, Ireland, France, and Austria [*Bailey et al.*, 2017]. We made improvements to the calculation of the electric field direction output of VW77's thin-sheet model, relative to previous European studies as described in Section 2.2. These improvements should increase the predictive power of GIC calculated using LP85's model compared to previous GIC modeling studies that used other methods to infer electric field direction from the thin-sheet model.

The GIC flowing to ground through each substation were calculated using LP85's technique. In an incremental improvement of the implementation of LP85's network model we have added the ability to represent parallel lines between the same nodes. This improvement is important to capture the full transmission network topography of New Zealand, the United Kingdom, and many other power networks. In the future the ability to calculate current through parallel lines will allow GIC researchers to test mitigation strategies that include switching off some redundant lines to increase the transmission resistance and hence hopefully contribute to procedures that reduce GIC impacts. Together, these improvements on the similar techniques used in European studies should be of interest to the wider GIC research community. Such an approach should be of interest to transmission network operators, and has been requested by Transpower NZ Ltd.

In further planned future work, driving the flow with a more realistic, spatially varying magnetic field as well as a more detailed network model may improve the agreement of our calculated GIC with observations. However, the gross patterns of spatial variability and strong GIC at ISL and BRY do match observations, giving further confidence that the electric field model yields a reasonable representation of the electric field around New Zealand, assuming a spatially uniform magnetic field. With further improvements to the network model allowing us to calculate the GIC through each individual transformer in the network, rather than only the GIC flowing to ground through each substation, we aim to validate the GIC network model against Transpower New Zealand Ltd's transformer level GIC observations [*Mac Manus et al.*, 2017] in a future study, as part of our ongoing 3 year research project. Transpower's GIC observations, collected since 2001 at up to 61 individual transformers, provide possibly the best GIC dataset in the world with which we will be able to formally validate our GIC modelling approach for the first time. As aspects of this approach have been used extensively in the wider GIC research community in the past, this future validation should provide a significant contribution to the GIC research and operational community. Once validated, this modeling approach will lead to a better understanding of GIC in New Zealand's South Island electrical transmission network and allow testing of mitigation strategies with the general aim of strengthening this power system against Space Weather.

Acknowledgments

The authors would like to thank Transpower New Zealand for supporting this study. This research was supported by the New Zealand Ministry of Business, Innovation and Employment Hazards and Infrastructure Research Fund Contract UOOX1502.

The South Island electrical transmission network's DC characteristics were provided to us by Transpower New Zealand with caveats and restrictions. This includes requirements of permission before all publications and presentations. In addition, we are unable to directly provide the full New Zealand network characteristics. Requests for access to these characteristics need to be made to Transpower New Zealand. At this time the contact point is Michael Dalzell (Michael.Dalzell@transpower.co.nz). We are very grateful for the substantial data access they have provided, noting this can be a challenge in the Space Weather field [*Hapgood and Knipp*, 2016].

References

Bailey, R. L., T. S. Halbedl, I. Schattauer, A. Römer, G. Achleitner, C. D. Beggan, V. Wesztergom, R. Egli, and R. Leonhardt (2017), Modelling geomagnetically induced currents in mid-latitude Central Europe using a thin-sheet approach, *Ann. Geophysicae*, *5*, 751–761, doi:10.5194/angeo-35-751-2017.

Beggan, C. D. (2015), Sensitivity of geomagnetically induced currents to varying auroral electrojet and conductivity models, *Earth, Planets and Space*, *67*(1), 24, doi: 10.1186/s40623-014-0168-9.

Beggan, C. D., D. Beamish, A. Richards, G. S. Kelly, and A. W. P. Thomson (2013), Prediction of extreme geomagnetically induced currents in the UK high-voltage network, *Space Weather*, *11*(7), 407–419, doi:10.1002/swe.20065.

Bertrand, E. A., T. G. Caldwell, G. J. Hill, E. L. Wallin, S. L. Bennie, N. Cozens, S. A. Onacha, G. A. Ryan, C. Walter, A. Zaino, and P. Wameyo (2012), Magnetotelluric imaging of upper-crustal convection plumes beneath the Taupo Volcanic Zone, New Zealand, *Geophysical Research Letters*, *39*(2), 6, doi:10.1029/2011GL050177.

Bertrand, E. A., T. G. Caldwell, G. J. Hill, S. L. Bennie, and S. Soengkono (2013), Magnetotelluric imaging of the Ohaaki geothermal system, New Zealand: implications for locating basement permeability., *Journal of Volcanology and Geothermal Research*, *268*, 36–45.

Blake, S. P., P. T. Gallagher, J. McCauley, A. G. Jones, C. Hogg, J. Campanyà, C. D. Beggan, A. W. P. Thomson, G. S. Kelly, and D. Bell (2016), Geomagnetically induced currents in the Irish power network during geomagnetic storms, *Space Weather*, *14*, 1–19, doi:10.1002/2016SW001534.

Bolduc, L. (2002), GIC observations and studies in the Hydro-Québec power system, *Journal of Atmospheric and Solar-Terrestrial Physics*, *64*(16), 1793–1802, doi:10.1016/S1364-6826(02)00128-1.

Bonner, L. R., and A. Schultz (2017), Rapid prediction of electric fields associated with geomagnetically induced currents in the presence of three-dimensional ground structure : Projection of remote magnetic observatory data through magnetotelluric impedance tensors, *Space Weather*, doi:10.1002/2016SW001535.

Boteler, D. H. (1994), Geomagnetically induced currents: present knowledge and future research, *IEEE Transactions on Power Delivery*, *9*(1), 50–58, doi:10.1109/61.277679.

Boteler, D. H., and R. J. Pirjola (1998), Modelling geomagnetically induced currents produced by realistic and uniform electric fields, *IEEE Transactions on Power Delivery*, *13*(4), 1303–1308, doi:10.1109/61.714500.

Boteler, D. H., and R. J. Pirjola (2014), Comparison of methods for modelling geomagnetically induced currents, *Annales Geophysicae*, *32*(9), 1177–1187, doi:10.5194/angeo-32-1177-2014.

Boteler, D. H., and R. J. Pirjola (2017), Modeling geomagnetically induced currents, *Space Weather*, *15*(1), 258–276, doi:10.1002/2016SW001499.

Bothmer, V., and I. A. Daglis (2007), *Space Weather- Physics and Effects*, Springer Berlin Heidelberg, Berlin, Heidelberg, doi:10.1007/978-3-540-34578-7.

Cassidy, J., M. Ingham, C. A. Locke, and H. M. Bibby (2009), Subsurface structure across the axis of the Tongariro Volcanic Centre, New Zealand., *Journal of Volcanology and*

Geothermal Research, *179*, 233–240.
Chamalaun, F., and D. McKnight (1993), A New Zealand wide magnetometer array study., *Journal of Geomagnetism and Geoelectricity*, *45*, 741–759.
Crane, A. T. (1990), *Physical vulnerability of electric systems to natural disaster and sabotage, OTA-E-453*, 66 pp., U.S. Government Printing Office, Washington, DC (USA).
Erinmez, I. A., J. G. Kappenman, and W. A. Radasky (2002), Management of the geomagnetically induced current risks on the national grid company's electric power transmission system, *Journal of Atmospheric and Solar-Terrestrial Physics*, *64*(5-6), 743–756, doi: 10.1016/S1364-6826(02)00036-6.
Gaunt, C. T., and G. Coetzee (2007), Transformer Failures in Regions Incorrectly Considered to have Low GIC-Risk, in *IEEE Lausanne*, p. 807, IEEE, Lausanne.
Gns.cri.nz (2015), Declination around New Zealand.
Gorman, P. (2012), Transpower battens down for sun storms.
Hapgood, M., and D. J. Knipp (2016), Data Citation and Availability: Striking a Balance Between the Ideal and the Practical, *Space Weather*, *14*(11), 919–920, doi: 10.1002/2016SW001553.
Heise, W., T. G. Caldwell, H. M. Bibby, and S. C. Bannister (2008), Three-dimensional modelling of magnetotelluric data from the Rotokawa geothermal field, Taupo Volcanic Zone, New Zealand, *Geophysical Journal International*, *173*(2), 740–750, doi:10.1111/j.1365-246X.2008.03737.x.
Heise, W., T. G. Caldwell, H. M. Bibby, and S. L. Bennie (2010), Three-dimensional electrical resistivity image of magma beneath an active continental rift, Taupo Volcanic Zone, New Zealand, *Geophysical Research Letters*, *37*(10), n/a–n/a, doi: 10.1029/2010GL043110.
Heise, W., T. G. Caldwell, G. J. Hill, S. L. Bennie, E. Wallin, and E. A. Bertrand (2012), Magnetotelluric imaging of fluid processes at the subduction interface of the Hikurangi margin, New Zealand, *Geophysical Research Letters*, *39*(4), n/a–n/a, doi: 10.1029/2011GL050150.
Heise, W., E. A. Bertrand, T. G. Caldwell, G. J. Hill, N. G. Palmer, and S. L. Bennie (2014), 2-D magnetotelluric imaging of the Rotorua and Waimangu geothermal fields, in *In Proceedings 36th New Zealand Geothermal Workshop, 24-26 November 2014, Auckland, New Zealand*, p. 2, University of Auckland, Auckland, N.Z.
Horton, R., D. Boteler, T. J. Overbye, R. Pirjola, and R. C. Dugan (2012), A Test Case for the Calculation of Geomagnetically Induced Currents, *IEEE Transactions on Power Delivery*, *27*(4), 2368–2373, doi:10.1109/TPWRD.2012.2206407.
Ingham, M. (1996), Magnetotelluric soundings across the South Island of New Zealand: electrical structure associated with the orogen of the Southern Alps, *Geophysical Journal International*, *124*(1), 134–148, doi:10.1111/j.1365-246X.1996.tb06358.x.
Ingham, M. (2005), Deep electrical structure of the Central Volcanic Region and Taupo Volcanic Zone, New Zealand, *Earth, Planets and Space*, *57*(7), 591–603, doi: 10.1186/BF03351838.
Ingham, M., K. Whaler, and D. McKnight (2001), Magnetotelluric sounding of the Hikurangi Margin, New Zealand, *Geophysical Journal International*, *144*(2), 343–355, doi: 10.1046/j.0956-540X.2000.01330.x.
Ingham, M. R. (1997), Electrical resistivity structure of the Canterbury Plains, New Zealand, *New Zealand Journal of Geology and Geophysics*, *40*(4), 465–471, doi: 10.1080/00288306.1997.9514776.
Ingham, M. R., H. M. Bibby, W. Heise, K. A. Jones, P. Cairns, S. Dravitzki, S. L. Bennie, T. G. Caldwell, and Y. Ogawa (2009), A magnetotelluric study of Mount Ruapehu volcano, New Zealand, *Geophysical Journal International*, *179*(2), 887–904, doi: 10.1111/j.1365-246X.2009.04317.x.
Kelly, G. S., A. Viljanen, C. D. Beggan, and A. W. P. Thomson (2017), Understanding GIC in the UK and French high-voltage transmission systems during severe magnetic storms, *Space Weather*, doi:10.1002/2016SW001469.

Kuvshinov, A. V. (2008), 3-D Global Induction in the Oceans and Solid Earth: Recent Progress in Modeling Magnetic and Electric Fields from Sources of Magnetospheric, Ionospheric and Oceanic Origin, *Surveys in Geophysics*, *29*(2), 139–186, doi: 10.1007/s10712-008-9045-z.

Lehtinen, M., and R. Pirjola (1985), Currents produced in earthed conductor networks by geomagnetically-induced electric fields, *Annales Geophysicae*, *3*(4), 479–484.

Liu, C.-M., L.-G. Liu, R. Pirjola, and Z.-Z. Wang (2009), Calculation of geomagnetically induced currents in mid- to low-latitude power grids based on the plane wave method: A preliminary case study, *Space Weather*, doi:doi:10.1029/2008SW000439.

Mac Manus, D. H., C. J. Rodger, M. Dalzell, A. W. P. Thomson, E. Clarke, M. A. Clilverd, T. Petersen, N. R. Thomson, and M. Wolf (2017), Long term Geomagnetically Induced Current Observations from New Zealand: Earth return Corrections and Comparison with Geomagnetic Field Driver, *Space Weather*, *In review*, doi:10.1002/2017SW001635.

Mackie, R. L., J. T. Smith, and T. R. Madden (1994), ThreeâĂŘdimensional electromagnetic modeling using finite difference equations: The magnetotelluric example, *Radio Science*, *29*(4), 923–935, doi:10.1029/94RS00326.

Marshall, R. A., M. Dalzell, C. L. Waters, P. Goldthorpe, and E. A. Smith (2012), Geomagnetically induced currents in the New Zealand power network, *Space Weather*, *10*(8), 8003, doi:10.1029/2012SW000806.

Marshall, R. A., H. Gorniak, T. Van Der Walt, C. L. Waters, M. D. Sciffer, M. Miller, M. Dalzell, T. Daly, G. Pouferis, G. Hesse, and P. Wilkinson (2013), Observations of geomagnetically induced currents in the Australian power network, *Space Weather*, *11*(1), 6–16, doi:10.1029/2012SW000849.

Mckay, A. J. (2003), PhD Thesis: Geoelectric Fields and Geomagnetically Induced Currents in the United Kingdom, Phd thesis, University of Edinburgh.

Mckay, A. J., and K. A. Whaler (2006), The electric field in northern England and southern Scotland: Implications for geomagnetically induced currents, *Geophysical Journal International*, *167*(2), 613–625, doi:10.1111/j.1365-246X.2006.03128.x.

McLoughlin, C., M. Ingham, K. Whaler, and D. McKnight (2002), A magnetotelluric transect of the Wairarapa region, New Zealand, *New Zealand Journal of Geology and Geophysics*, *45*(2), 257–269, doi:10.1080/00288306.2002.9514972.

Parkinson, W. D. (1962), The Infiuence of Continents and Oceans on Geomagnetic Variation, *Geophysical Journal of the Royal Astronomical Society*, *6*(4), 441–449, doi: https://doi.org/10.1111/j.1365-246X.1962.tb02992.x.

Parkinson, W. D., and F. W. Jones (1979), The Geomagnetic Coast Effect, *Review of Geophysics*, *17*(8), 1999–2015, doi:10.1029/RG017i008p01999.

Pringle, D., M. Ingham, D. McKnight, and F. Chamalaun (2000), Magnetovariational soundings across the South Island of New Zealand: difference induction arrows and the Southern Alps conductor, *Physics of the Earth and Planetary Interiors*, *119*(3-4), 285–298, doi: 10.1016/S0031-9201(99)00173-9.

Pulkkinen, A. (2015), Geomagnetically Induced Currents Modeling and Forecasting, *Space Weather*, *13*(11), 734–736, doi:10.1002/2015SW001316.

Püthe, C., and A. Kuvshinov (2013), Towards quantitative assessment of the hazard from space weather. Global 3-D modellings of the electric field induced by a realistic geomagnetic storm, *Earth, Planets and Space*, *65*(9), 1017–1025, doi:10.5047/eps.2013.03.003.

Püthe, C., C. Manoj, and A. Kuvshinov (2014), Reproducing electric field observations during magnetic storms by means of rigorous 3-D modelling and distortion matrix co-estimation, *Earth, Planets and Space*, *66*, 1–10, doi:10.1186/s40623-014-0162-2.

Richardson, G., and C. Beggan (2017), Validation of geomagnetically induced current modelling code, Technical Report IR/17/009, *Tech. rep.*, British Geological Survey.

Stagpoole, V., S. Bennie, H. Bibby, S. Dravitzki, and M. Ingham (2009), Deep structure of a major subduction back thrust: Magneto-telluric investigations of the Taranaki Fault, New Zealand, *Tectonophysics*, *463*(1-4), 77–85, doi:10.1016/j.tecto.2008.09.035.

Thomson, A. W. P., A. J. McKay, E. Clarke, and S. J. Reay (2005), Surface electric fields and geomagnetically induced currents in the Scottish Power grid during the 30 October 2003 geomagnetic storm, *Space Weather*, *3*(11), 1–14, doi:10.1029/2005SW000156.

Torta, J. M., L. Serrano, J. R. Regué, A. M. Sánchez, and E. Roldán (2012), Geomagnetically induced currents in a power grid of northeastern Spain, *Space Weather*, *10*(6), 1–11, doi:10.1029/2012SW000793.

Trivedi, N. B., Í. Vitorello, W. Kabata, S. L. G. Dutra, A. L. Padilha, M. S. Bologna, M. B. de Pádua, A. P. Soares, G. S. Luz, F. d. A. Pinto, R. Pirjola, and A. Viljanen (2007), Geomagnetically induced currents in an electric power transmission system at low latitudes in Brazil: A case study, *Space Weather*, *5*(4), n/a–n/a, doi:10.1029/2006SW000282.

Uyeshima, M., and A. Schultz (2000), Geoelectromagnetic induction in a heterogeneous sphere: a new three-dimensional forward solver using a conservative staggered-grid finite difference method, *Geophys. J. Int*, *140*, 636–650.

Vasseur, G., and P. Weidelt (1977), Bimodal electromagnetic induction in non-uniform thin sheets with an application to the northern Pyrenean induction anomaly, *Geophysical Journal International*, *51*(3), 669–690, doi:10.1111/j.1365-246X.1977.tb04213.x.

Wannamaker, P. E., G. R. Jiracek, J. A. Stodt, T. G. Caldwell, V. M. Gonzalez, J. D. McKnight, and A. D. Porter (2002), Fluid generation and pathways beneath an active compressional orogen, the New Zealand Southern Alps, inferred from magnetotelluric data, *Journal of Geophysical Research*, *107*(B6), 1–20, doi:10.1029/2001JB000186.

Wannamaker, P. E., T. G. Caldwell, G. R. Jiracek, V. Maris, G. J. Hill, Y. Ogawa, H. M. Bibby, S. L. Bennie, and W. Heise (2009), Fluid and deformation regime of an advancing subduction system at Marlborough, New Zealand, *Nature*, *460*(7256), 733–736, doi:10.1038/nature08204.

Whittaker, J. M., A. Goncharov, S. E. Williams, R. D. Müller, and G. Leitchenkov (2013), Global sediment thickness data set updated for the Australian-Antarctic Southern Ocean, *Geochemistry, Geophysics, Geosystems*, *14*(8), 3297–3305, doi:10.1002/ggge.20181.

Wiese, H. (1962), Geomagnetische Tiefentellurik Teil II: Die Streichrichtung der untergrundstrukturen des elektrischen Widerstandes, erschlossen aus geomagnetischen Variationen, *Geofisica Pura e Applicata*, *52*(1), 83–103, doi:10.1007/BF01996002.